View metadata, citation and similar papers at core.ac.uk
brought to you by CORE
provided by CiteSeerX

Proceedings of IMECE2002
ASME International Mechanical Engineering Congress & Exposition
November 17–22, 2002, New Orleans, Louisiana

IMECE2002-33615

ADAPTIVE FEEDRATE SCHEDULING AND MATERIAL ENGAGEMENT ANALYSIS FOR HIGH PERFORMANCE MACHINING

Jirawan Kloypayan

Department of Industrial Engineering
North Carolina State University
Raleigh, NC 27695-7906
U. S. A.

Yuan-Shin Lee*

Department of Industrial Engineering
North Carolina State University
Raleigh, NC 27695-7906
U. S. A.

*: To whom the correspondence should be addressed

ABSTRACT

This paper presents a technique of feedrate scheduling by analyzing the material removal volume when a tool moves in linear, circular, or parametric curved motions. Tool motions of different types of endmilling cutters are considered in this study. By studying the relationship between the cutter geometry and the tool motion, the material removal rates of different cutters are analyzed. The adaptive feedrate scheduling can be determined to maintain a constant cutting load. The technique developed in this research can be used for tool path generation in CAD/CAM systems for 2.5D NC machining.

Keywords: adaptive feedrate scheduling, material removal volume, high speed machining, 2.5D pocket milling

INTRODUCTION

In milling processes, the cutting force on the cutter varies due to the change of the engaged removal material volume, as shown in Figure 1. The change of material removal rate in milling processes may cause tool breakage or damage the machined part surface [21]. This problem becomes even more severe when the cutting speed becomes higher. For example, in high speed machining (HSM), a slight change of cutting direction may cause significant increase of cutting force, which may damage the part surfaces and/or cutters [20]. To apply high speed machining and avoid tool breakage, understanding the tool's removal volume engagement and changing tool paths in machining is an important issue.

When a tool moves into different regions or changes its cutting direction, the engage angle and the swept volume are changed [22]. As shown in Figure 1, an engage angle (a_b) is defined as the angle at the cutting edge between the start and finish locations of the material engagement [19]. Figure 1 shows the different engage angles (a_b) of a cutter moving in different cutting tool paths. In Figure 1, *s* is the cutting step-over distance. Figure 1(a) shows the engage angle a_{b0} of a cutter moving in linear tool motion. Figure 1(b) shows the increase of engage angle a_{b1} when the cutter moves into a corner ($a_{b1} > a_{b0}$). When a tool moves in the convex motion,

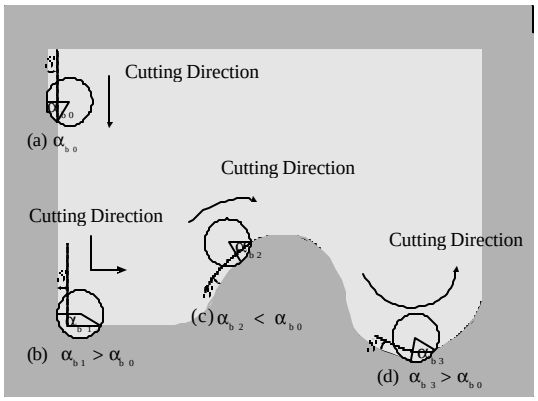

(a) Engage angle α_{b0}, in linear tool motion,
(b) Cutter moves into a corner, $\alpha_{b1} > \alpha_{b0}$
(c) In convex tool motion, $\alpha_{b2} < \alpha_{b0}$
(d) In concave tool motion, $\alpha_{b3} > \alpha_{b0}$

Figure 1. Changes of engage angle a_b due to different types of tool motions

the engage angle a_{b2} is less than a_{b0} of linear motion ($a_{b2} < a_{b0}$), as shown in Figure 1(c). For the concave circular tool motion in Figure 1(d), the engage angle a_{b3} in the concave region has a larger value than a_{b0} of the linear tool motion ($a_{b3} > a_{b0}$). Changing the engage angle along different tool path trajectories causes the variation of the cutting load [19, 20]. The reduction of the feedrate is expected to reduce the actual chip overload and consequently increase the tool life [2]. Furthermore, reduced variations of the cutting force can improve the machining accuracy and surface finish [5]. The

Copyright © 2002 by ASME

Downloaded From: https://proceedings.asmedigitalcollection.asme.org on 06/29/2019 Terms of Use: http://www.asme.org/about-asme/terms-of-use

cutting forces are proportional to instantaneous material removal rate, which can have different instantaneous peak values [9]. To maintain constant material engagement or maintain the material removal rate may reduce the peak forces variation.

Many researchers studied the relationship among the cutting force, chip thickness, engage angle and material removal rate. Tsai [22] developed a method to control the instantaneous engage angle by modifying the tool path at the circular path segment and adding additional tool path segments at the corner. Stori [20] introduced a new offset algorithm to maintain a constant engagement tool path for convex curves. Wang [24] and Kramer [14] studied the relationship between the material removal rate and feedrate parameters for milling using a flat-endmill. Bailey [1] developed a process simulator for selecting cutting conditions to maximize the material removal rate subject to cutting force, power, and chip load constraints. Rodriguez [19] studied the relationship between the chip thickness and the machining parameters such as feedrate and cutting speed to maintain a desired cutting load. His method considered only the linear cutting motions. Ip [8] and Huang [7] used the fuzzy logic method to increase material removal rate and to maintain a constant cutting load. According to the literature, most of the research was focused on studying the linear tool motion or only on flat-endmill cutting. Very little work has been reported on studying the use of different types of endmill cutters in machining or different types of tool motions, for example B-spline tool paths.

In this paper, the geometric models and detailed formulation of material removal volumes are studied for different types of endmilling cutters in a variety of cutting tool motions. The generalized cutter geometry, which is capable of representing different types of endmilling cutters (ball-endmills, flat-endmills, fillet-endmills and taper endmills), is used in this study [11]. The geometric models and formulae of material removal rates presented in this paper can be used for adaptive feedrate control with constant cutting load. The adaptive feedrate scheduling is determined to maintain a constant material removal rate, which result in constant cutting load along tool paths. This is especially useful in machining curved part surfaces and in high speed machining for a constant cutting force.

2 GENERALIZED CUTTER GEOMETRY OF DIFFERENT ENDMILLS

In this section, the generalized cutter geometry for different types of endmills (including flat-endmill, ball-endmill, fillet-endmill and taper-endmill) is introduced. Different types of endmills generate different surface marks in machining due to the difference of cutters' geometries [4, 14]. Figure 2 shows the generalized cutter geometry based on the APT (Automated Programming Tool) definition [13]. As shown in Figure 2, the definitions of the geometric parameters are shown as follows:

- r : cutter radius,
- r_{tc} : radius of the corner circle; it can be zero or no larger than r,
- e: radial distance from the tool axis to the center of the corner circle,
- h : cutter height measured from the tool endpoint along the tool axis,
- h_{tc}: distance from the tool endpoint to the center of the corner circle measured parallel to the tool axis,
- b_t : angle between the upper segment and the tool axis, and $-90^{o} < b_t < 90^{o}$,
- d_t : angle from a radial line through the tool endpoint to the lower line segment, and $0^{0} \le d_t < 90^{0}$.

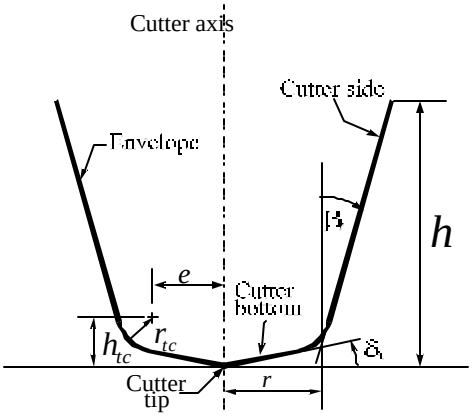

Figure 2. Generalized cutter geometry definition (Based on the APT definition [13].)

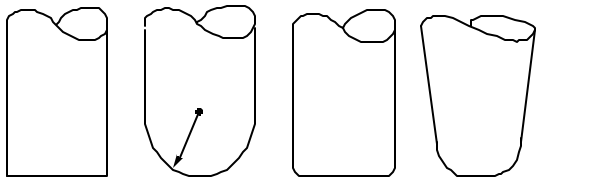

(a) Flat-endmill (b) Ball-endmill (c) Fillet-endmill (d) Taper-endmill

Figure 3. Different types of endmills [4]

In this paper, four different types of endmill cutters, which include flat-endmill, ball-endmill, fillet-endmill and taper-endmill (as shown in Figure 3), are considered. Detailed discussion of the APT tool geometry and the geometric variables has been presented in our earlier work in [4, 11]. By considering the cutter geometry and the material engagement, the material removal volume for different endmills in machining can be determined. The detailed formulations of the cutting cross-sections for different types of endmills are presented in the next section.

3 ANALYSIS OF CUTTING CROSS-SECTION AREAS FOR DIFFERENT ENDMILLS

To analyze the material removal volumes of cutters moving along different paths, the cutting cross-section areas of endmill cutters must be determined. Figure 4 shows a cutter machining a part surface. To calculate the cutting cross-section areas of different endmills, a more complex cutter geometry (for example, a generalized cutter or a taper-endmill) is used. Once the geometric model of cutting cross-section area for a generalized cutter is formulated, other simpler cutters (for example, flat-endmill or ball-endmill) are actually special cases of the generalized cutter geometry model. The cutting cross-section information can be used to calculate the material removal rate, which will be discussed later in Section 4.

Copyright © 2002 by ASME

Downloaded From: https://proceedings.asmedigitalcollection.asme.org on 06/29/2019 Terms of Use: http://www.asme.org/about-asme/terms-of-use

3.1 Cutting cross-section of the generalized cutters

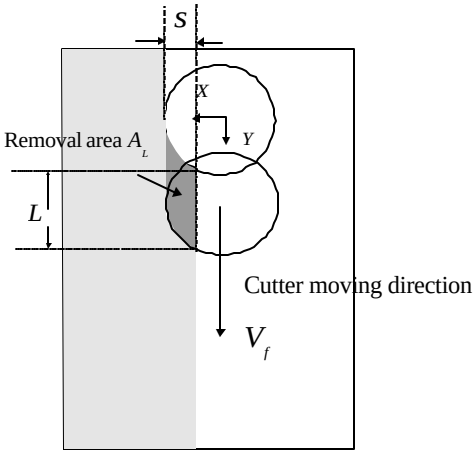

(a) Top view and removal area A_L

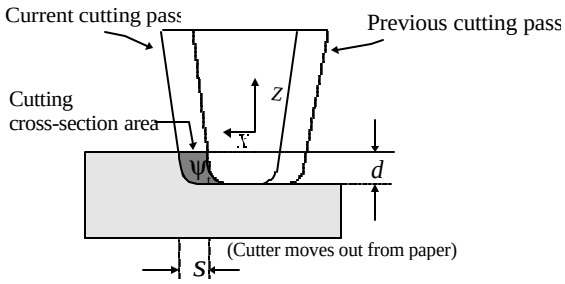

y_t is cutting cross-section area for a taper-endmill, s is the step over distance, d is the depth of cut.

(b) Front view and cutting cross-section y_t

Figure 4. Cutting cross-section y_t for a taper-endmill machining a part

Figure 4 shows the cutting cross-section y_t when a part surface is machined by using a taper-endmill. The cutter axis is parallel to Z-axis and the cutter is moving on the X-Y plane. Figure 4(a) shows the top view (X-Y plane) of a cutter, and the cutter is moving along the Y-axis. In Figure 4(a), L is the distance of the cutter moving from the previous cutter location to the next one within a given time T with a feedrate V_f. The dark area A_L in Figure 4(a) is the removal area on part surface when the endmill cutter advances with a distance L during a period of time T. The material removal volume under A_L can be found by multiplying the cutting cross-section area y_t and the cutter advance distance L, as shown in Figure 4(a). Figure 4(b) shows the front view of the cutter and the step over distance s between two adjacent cutting passes. The dark area y_t in Figure 4(b) represents the cutting cross-section area y_t of material removed with a taper-endmill in machining.

To find the area of the complex cutting cross-section, the complex cross-section is divided into a set of manageable sub-areas as shown in Figure 5. For a cross-section area y_G of a generalized cutter, the total area can be calculated as follows (Figure 5(b)):

$$y_G = \sum_{i=1}^{n} y_i \tag{1}$$

where y_i is the sub-area of the cutting cross-section y_G.

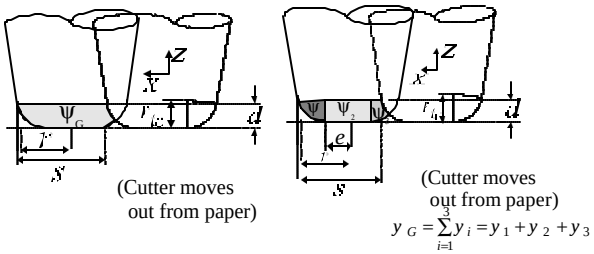

(a) Area of cutting cross-section b) Dividing the cross-section area into a set of sub-areas.

Figure 5. The cutting cross-section area y_G

After finding each of the sub-area y_i, the total area y_G of a generalized cutter is calculated by using Equation (1). The cutting cross-section area y_G of a generalized cutter can be found as follows:

For $s > 2e$,

$$y_G = \frac{r_{tc}^2(p - 2f) + 2r_{tc}^2 \sin f \cos f + 4r_{tc}e + 2s(d - r_{tc})}{2} \tag{2}$$

For $s \le 2e$,

$$y_G = s \cdot d \tag{3}$$

where $f = \cos^{-1}[(s - 2e)/2r_{tc}]$ and d is the depth of cut.

Detailed calculation of the sub-area of a generalized cutter can be found in our earlier work presented in [12]. The cutting cross-section area y_G of a generalized cutter from Equations (2) and (3) will be used to determine the adaptive feedrate control in Section 4.

3.2 Cutting cross-section areas of different cutters

Figure 6 shows the cutting cross-section areas of different endmills. Figure 6(a) shows the cutting cross-section y_{fil} of a fillet-endmill in machining process. The cutter is moving along the Y-axis on the X-Y plane (i.e., cutter moves out from paper in Figure 6). The material removal cross-section area y_{fil} can be calculated by using the generalized Equations (2) and (3) and the cutter's geometric parameters (Figure 3), depending on the step-over distance s.

Figure 6(b) shows the cutting cross-section y_f of a flat-endmill when the cutter is machining a workpiece. For a flat-endmill, the angle f and corner radius r_{tc} are both equal to zero, as discussed earlier in Figure 3. By substituting (f = 0.0) and (r_{tc}= 0.0) into Equations (2) and (3), we can find y_f of a flat-endmill, shown as follows (Figure 6(b)):

$$y_f = s \cdot d \tag{4}$$

Copyright © 2002 by ASME

Downloaded From: https://proceedings.asmedigitalcollection.asme.org on 06/29/2019 Terms of Use: http://www.asme.org/about-asme/terms-of-use

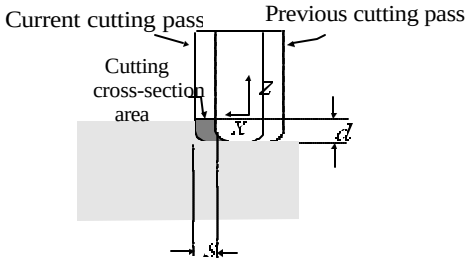

(a) Fillet-endmill y_{fil}

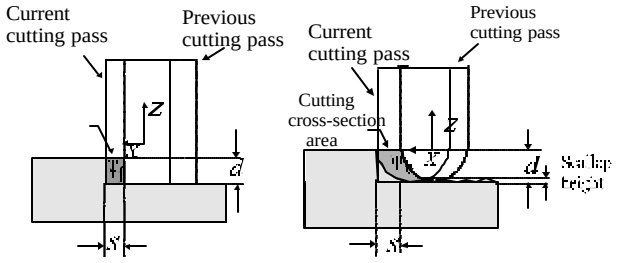

(b) Flat-endmill y_f (c) Ball-endmill y_b

Figure 6. Cutting cross-section y for fillet-endmills, flat-endmills, and ball-endmills

Figure 6(c) shows the cutting cross-section y_b of a ball-endmill machining a workpiece. Ball-endmill cutters are usually used to machine curved surfaces. Using ball-endmill cutters in machining, cusps are left on the machined surface after machining [16]. The height of the cusp depends on the step-over distance *s*. The larger the step-over distance *s* is, the higher the scallop height becomes [15]. The dark area y_b in Figure 6(c) represents the cutting cross-section area y_b of the removed material when a ball-endmill is machining a part surface. For a ball-endmill, the corner radius r_{tc} is equal to the cutter radius r ($r_{tc}=r$), as shown earlier in Figure 3. Substituting ($r_{tc}=r$) into Equation (2), the cutting cross-section y_b of ball-endmills can be found as follows (Figure 6(c)):

$$y_b = \frac{r^2(p-2f)+2r^2\sin f\cos f+2s(d-r)}{2} \qquad (5)$$

where $f=\cos^{-1}(s/2r)$. Using Equations (2), (3), (4) and (5), the material removal volumes of different endmills can be found for cutters moving along a variety of tool paths.

4 MATERIAL REMOVAL RATE ANALYSIS FOR DIFFERENT TOOL MOTIONS

The material removal rate (MRR) can be calculated by using the cutting cross-sectional area y_G, feedrate and the cutting tool motions. In this section, we formulate the relationship between the material removal rate and the feedrate when a tool moves in either linear or curved motion.

4.1 Centroids of cutting cross-sections for different cutters in machining

As shown in Figure 4, when a cutter is moving along a linear motion, the removed material volume is equal to the swept volume generated by the cross-section area y_G along the linear tool trajectory. The material removal rate (MRR) of a cutter moving along a linear trajectory can be calculated as follows:

$$MRR = y_G \cdot V_f \qquad (6)$$

where $y_G = \begin{cases} y_f & : when\ the\ tool\ is\ a\ flat-endmill \\ y_b & : when\ the\ tool\ is\ a\ ball-endmill \\ y_{fil} & : when\ the\ tool\ is\ a\ fillet-endmill \\ y_t & : when\ the\ tool\ is\ a\ taper-endmill \end{cases}$ and

V_f is the feedrate of the cutter moving in linear motion.

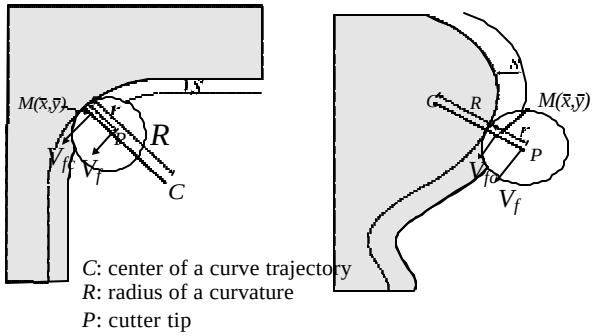

(a) A cutter moves along a concave surface (b) A cutter moves along a convex surface

Figure 7. The material engagement and the feedrate in circular motion

The cutting cross-section y_G in Equation (6) can be found by using Equations (2) and (3). Figure 7 shows a cutter moving along a curve trajectory with a radius of curvature *R*, and *C* is the center of the curve trajectory. When a cutter moves along a curve path with a radius of curvature *R*, the material removal rate can be found as the cross-section area y_G multiplies by the corresponding feedrate V_{fc} at the "centroid" of the cutting cross-section [14]. Since the feedrate V_f is defined at the cutter tip, the corresponding feedrate V_{fc} is the proportional feedrate calculated at the centroid of the cross-section area y_G, as shown in Figure 7. The term "centroid" is defined as the location in a set of physical bodies where the total mass can be conceived to be concentrated [18]. The moment of the concentrated mass with respect to any axis or plane is equal to the moment of the distributed mass with respect to the same axis or plane. In a homogeneous body, the centroid and the mass center are at the same position. In this paper, we assume the workpiece is homogeneous and the centroid is the same as the mass center of the cutting removal volume.

On the cutting cross-section plane, we use the coordinates $M(\bar{x},\bar{y})$ to represent the centroid of the area y_G on the plane. The total cross-section area y_G of a generalized endmill consists of a set of sub-areas: $\{y_1, y_2, y_3, \ldots, y_n\}$. The centroid $M(\bar{x},\bar{y})$ is calculated by using $(\bar{x}_i,\bar{y}_i)$ of each sub-area of $\{y_1, y_2, y_3, \ldots, y_n\}$ as follows:

$$M(\bar{x},\bar{y}) = \frac{\sum_{i=1}^{n} y_i \cdot (\bar{x}_i,\bar{y}_i)}{y_G} \qquad (7)$$

where y_i is the sub-area of $\{y_1, y_2, \ldots, y_n\}$, y_G is the total cutting cross-section area of y_i, i = 1,2,...,n.

Copyright © 2002 by ASME

Downloaded From: https://proceedings.asmedigitalcollection.asme.org on 06/29/2019 Terms of Use: http://www.asme.org/about-asme/terms-of-use

The centroid $(\bar{x}_i, \bar{y}_i)$ of each sub-area y_i can be calculated as follows [18]:

$$\bar{x}_i = \frac{\iint x\,dxdy}{y_i} \tag{8}$$

$$\bar{y}_i = \frac{\iint y\,dydx}{y_i} \tag{9}$$

The centroid coordinates $(\bar{x}_i, \bar{y}_i)$ of the sub-areas y_i are dependent on the step-over distance *s* and the radial distance *e*. As presented in our earlier work in [12], the centroid coordinates $M_G(\bar{x}, \bar{y})$ of a generalized endmill can be calculated as follows:

When $d > r_{tc} - r_{tc}\sin\Omega$

$$M_{G,d>r_{tc}}(\bar{x},\bar{y}) = \frac{\left|(\bar{x}_1,\bar{y}_1)*y_1 + (\bar{x}_2,\bar{y}_2)*y_2 + (\bar{x}_3,\bar{y}_3)*y_3 + (\bar{x}_4,\bar{y}_4)*y_4\right|}{y_G} \tag{10}$$

and, when $d \le r_{tc} - r_{tc}\sin\Omega$

$$M_{G,d\le r_{tc}}(\bar{x},\bar{y}) = \frac{\left|(\bar{x}_2,\bar{y}_2)*y_2 + (\bar{x}_3,\bar{y}_3)*y_3 + (\bar{x}_4,\bar{y}_4)*y_4\right|}{y_G} \tag{11}$$

In Equations (10) and (11), the angle can be found to be $\Omega = \cos^{-1}\left(r_{tc}/((r-e) + r_{tc}\tan b)\right)$. The details of different cutting cross-section areas for a taper-endmill, ball-endmill and fillet-endmill were discussed in our earlier work in [12].

4.2 Determination of the adaptive feedrate control

As shown in Figure 7, when a cutter moves along a curved path, the center *C* of the curvature and the radius *R* of the curvature can be found. Since the feedrate *V* is defined at the cutter tip *P*, the corresponding feedrate V_{fc} at the centroid $M(\bar{x}, \bar{y})$ of the cutting cross-section y_G needs to be found. Due to the circular motion of the cutter, the corresponding feedrate V_{fc} at the centroid $M(\bar{x}, \bar{y})$ can be found to be proportional to the feedrate *V* at the cutter tip P, as shown in Figure 7. In Figure 7(a), a cutter is moving along a concave surface and the corresponding feedrate V_{fc} at the centroid $M(\bar{x}, \bar{y})$ of the cutting cross-section y_G can be found as follows:

$$V_{fc,cv} = \frac{V_f \cdot (R - \bar{m})}{(R - r)} \tag{12}$$

where V_f is the feedrate at the cutter tip *P*, $\bar{m} = \sqrt{(\bar{x})^2 + (\bar{y})^2}$, *R* is the radius of curvature, *r* is the cutter radius, and $(\bar{x}, \bar{y})$ are the coordinates measured from the cutter contact point.

Figure 7(b) shows a cutter is moving along a convex surface and the corresponding feedrate V_{fc} at the centroid $M(\bar{x}, \bar{y})$ of the cutting cross-section?y_G can be calculated as follows:

$$V_{fc,cx} = \frac{V_f \cdot (R + \bar{m})}{(R + r)} \tag{13}$$

Using Equations (12) and (13), we can find the corresponding feedrate V_{fc} at the centroid $M(\bar{x}, \bar{y})$ of a cutter moving along a curved path. The material removal rate of a cutter moving along a curved path can be formulated as the corresponding feedrate V_{fc} multiplied with the cross-section area y_G, shown as follows:

$$MRR = y_G \cdot V_{fc} \tag{14}$$

where V_{fc} is the corresponding feedrate at the centroid of y_G. By using Equations (12), (13) and (14), we can summarize the MRR formulation of a cutter moving along the convex or the concave paths as follows:

$$MRR_{cx} = \frac{y_G \cdot V_f \cdot (R + \bar{m})}{(R + r)}, \quad \text{for convex paths} \tag{15}$$

$$MRR_{cv} = \frac{y_G \cdot V_f \cdot (R - \bar{m})}{(R - r)}, \quad \text{for concave paths.} \tag{16}$$

In NC part programming, the rotational speed *N* (rpm) can be determined based on the maximum cutting speed *v* (ipm) and the cutter diameter *D* by using the following equation [11]:

$$v = p \cdot D \cdot N \tag{17}$$

The tangential cutting force *F* of a cutter in linear motion can be calculated by using the MRR and the cutting speed *v* as follows [8]:

$$F_{linear} = \frac{MRR \cdot E}{v}, \quad \text{for linear tool motion} \tag{18}$$

where *E* is the specific energy of the part material. To find the tangential cutting force *F* of a cutter moving along a curved tool path, the cutting force *F* can be found by substituting Equations (15) and (16) into Equation (18) as follows:

$$F_{cx} = \frac{y_G \cdot V_f \cdot (R + \bar{m}) \cdot E}{v \cdot (R + r)}, \text{ for a convex path} \tag{19}$$

and,

$$F_{cv} = \frac{y_G \cdot V_f \cdot (R - \bar{m}) \cdot E}{v \cdot (R - r)}, \text{for a concave path} \tag{20}$$

where *E* is the specific energy of the part material. To maintain a constant cutting force *F*, the material removal rate (MRR) in Equation (18) needs to be maintained as a constant no matter whether the cutter is moving in a linear motion or along a curved path. To maintain a smooth MRR along a curved path, the corresponding feedrate V_{fc} at the centroid $M(\bar{x}, \bar{y})$ of the cutter needs to be adaptively determined. In the current tool path generation method, the feedrate V_f is determined at the cutter tip [17]. To keep the corresponding feedrate V_{fc} at the centroid $M(\bar{x}, \bar{y})$ constant, we can determine the adaptive feedrate V_{adp} at the cutter tip as follows:

$$V_{adp,cx} = \frac{V_{fc}(R + r)}{(R + \bar{m})}, \text{ for a convex path} \tag{21}$$

Copyright © 2002 by ASME

Downloaded From: https://proceedings.asmedigitalcollection.asme.org on 06/29/2019 Terms of Use: http://www.asme.org/about-asme/terms-of-use

$$V_{adp,cv} = \frac{V_{fc}(R-r)}{(R-\overline{m})}, \text{ for a concave path} \quad (22)$$

$$V_{adp,linear} = V_{fc}, \text{ for a linear path} \quad (23)$$

where V_{fc} is the corresponding feedrate at the centroid of cutting cross-section y_G, R is the radius of the curvature, r is the cutter radius, and $\overline{m} = \sqrt{(\overline{x})^2 + (\overline{y})^2}$, measured from the cutter contact point.

By using Equations (21), (22) and (23), we can determine the adaptive feedrate V_{adp} of a cutter moving along curved paths or linear paths for the smoothened cutting load and MRR in machining. To verify the feasibility of the adaptive feedrate control, it is also of interest to know the tool motion acceleration of the machine tools. The maximum acceleration of the conventional machine tools is ranging between 0.2-0.3G (i.e., 77-115.7 inches/sec^2, with 1G = 385.8 inches/sec^2) [10]. For the new high speed machine tools, an acceleration of 1G (385.8 inches/sec^2) or higher can be easily achieved [10]. In this paper, the machine tool tangential acceleration, a, is found as follows [6]:

$$a = \frac{\Delta f}{\Delta t} = \frac{f_{i+1} - f_i}{t_{i+1} - t_i} = \frac{\left(f_{i+1}^2 - f_i^2\right)}{2 \cdot \left(l_{i+1} - l_i\right)} \quad (24)$$

where $\Delta t = \frac{l_{i+1} - l_i}{\left(\frac{f_{i+1} + f_i}{2}\right)} = \frac{2 \cdot \left(l_{i+1} - l_i\right)}{\left(f_{i+1} + f_i\right)}$, l_i, l_{i+1} are the arc length at time t_i, t_{i+1} with feedrate f_i and f_{i+1}, respectively.

The computer implementation of the presented techniques and the illustrative examples are shown in next section.

5 COMPUTER IMPLEMENTATION AND EXAMPLES

The methods presented in this paper have been implemented on 200 MHz computer workstations using MATLAB® software. Several illustrative examples are presented in this section to demonstrate the feasibility of the developed techniques.

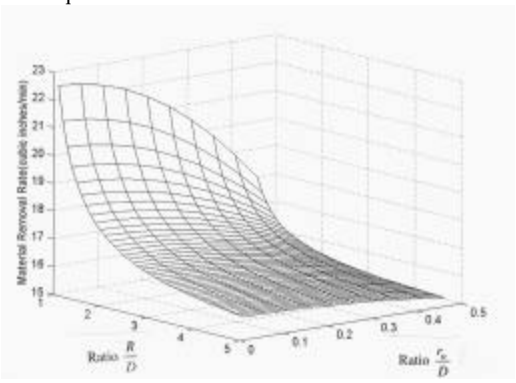

Cutter diameter D = 1.0", Depth of cut d = 0.3", Step-over distance s = 0.5", Radius of curved path R, Corner radius of cutter r_{tc}

Figure 8. The relationship of the MRR and the ratio of R/D and the ratio of r_{tc}/D

Figure 8 shows the relationship among the material removal rate, the radius of curved path R and the corner radius r_{tc}. In Figure 8, a cutter diameter D=1.0″, depth of cut d = 0.3″, step-over distance s = 0.5″ and a selected feedrate V_f = 100 ipm are used for demonstration. In Figure 8, when the ratio of (R/D) is increased, the tool path becomes less "curved" (i.e., more "linear") and the material removal rate becomes smaller. The ratio (r_{tc}/D) indicates the different shapes of the cutters. As discussed earlier (in Figure 3), when $(r_{tc}/D) = 0.0$, the cutter is a flat-endmill. When $(r_{tc}/D) = 0.5$, the cutter is a ball-endmill. When $0.0 < (r_{tc}/D) < 0.5$, it is a fillet-endmill. As shown in Figure 8, when (r_{tc}/D) is increased (i.e., more like "ball-endmill" shape), the material removal rate is decreased, which is consistent with the earlier observation of flat-endmills having higher MRR than ball-endmill presented in [23].

Figure 9(a) shows an example of a part surface that has rectangular corners (angle = 90 degree). The solid line is a part surface and the dash line represents the offset tool path trajectory. Figure 9(b) shows the calculated material removal rate MRR when a tool moves into the corner and changes its direction. At each corner, there is an uncut area (i.e., shaded area in Figure 9(a)) left from the previous cutting pass. This will cause the increasing of cutting material engagement, as shown in Figure 9(b). When a tool reaches a corner, the MRR gradually increases at the beginning (due to the uncut area left by the previous cutting pass), and then increases vastly because of the larger engage angle, as discussed earlier in Figure 1(b). After the cutter changes to the new cutting direction and moves in a linear motion, the MRR returns to the normal MRR, as shown in Figure 9(b).

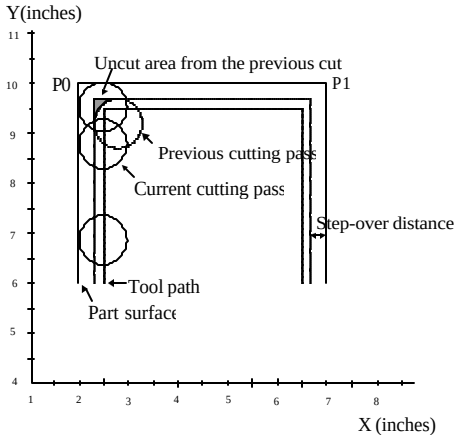

(a) Example part surface with rectangular corner and the tool path for machining

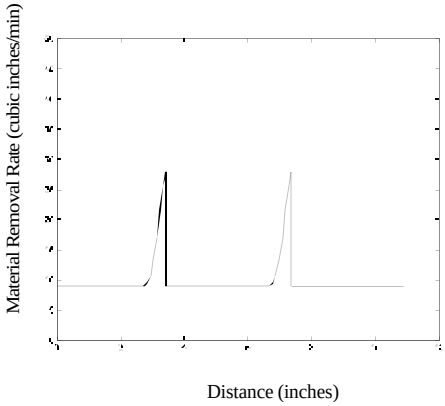

(b) Calculated material removal rate along the tool path

Figure 9. The material removal rate along the example

Copyright © 2002 by ASME

Downloaded From: https://proceedings.asmedigitalcollection.asme.org on 06/29/2019 Terms of Use: http://www.asme.org/about-asme/terms-of-use

Figure 10 shows an example pocket part bounded by a curved boundary. The pocket part surface shown in Figure 10 is machined by using an endmill of cutter radius r = 0.5". The step-over distance s is 0.5" and the depth of cut d is 0.3". The correspondence feedrate V_{fc} at the centroid is kept constant at 100 ipm. Figure 11 shows the generated tool path for machining the example pocket part surface by using contour method in Unigraphics® software package. Figure 12 shows the material engagement and the adaptive feedrate (V_{adp}) control along the tool path for machining the example part. Different types of endmill, including taper-endmill (with 30^o angle), flat-endmill, fillet-endmill and ball-endmill, are used in the same example, as shown in Figutr 12(a). When the

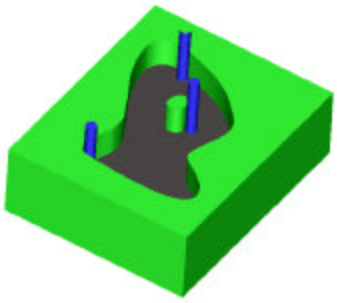

Figure 10. Example part surface with a free-form pocket boundary

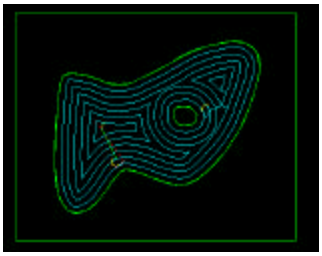

Figure 11. The tool path for machining the example pocket

cutter is machining along the curved boundary, the material removal rate MRR at the concave region has a higher value than the MRR at the convex region, as shown in Figure 12(a). This is due to the fact that the corresponding feedrate V_{fc} has a larger value than the feedrate V_f at cutter center when the cutter is moving along curved paths, as shown earlier in Equations (12) and (13). Notice that, given the same cutting condition and cutter size, the taper-endmill generally has the highest MRR, following by the flat-endmill and fillet-endmill, and the ball-endmill usually has a smaller MRR, as shown in Figure 12(a). To maintain a constant cutting load along curved tool paths, the adaptive feedrate V_{adp} at the cutter center needs to be calculated by using Equations (21), (22) and (23), as discussed earlier in Section 4. Figure 12(b) shows the adaptive feedrate (V_{adp}) based on the constant material engagement along the curved tool path while machining the free-form boundary of the example part surface in Figure 10.

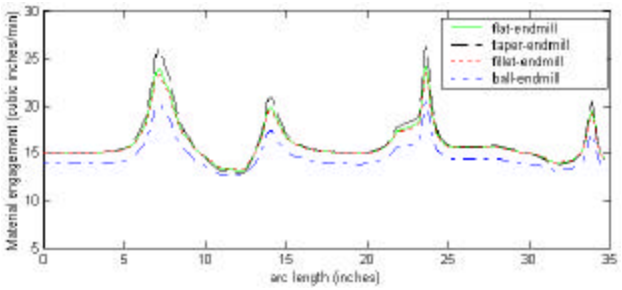

(a) Calculated material removal rate along the curved path

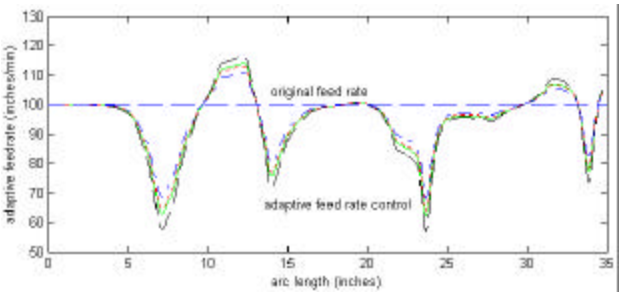

(b) Calculated adaptive feedrate V_{adp}

Figure 12. The material engagement and the adaptive feedrate control for machining the example part (using flat-endmill, taper-endmill, fillet-endmill and ball-endmill)

Figure 13 shows an example pocket with taper boundary surfaces. The example part has two levels of pockets with the inclined boundary surfaces (of 30^o inclination angle), as shown in Figure 13(a). Figures 13(b) and 13(c) show the generated tool path for machining the upper pocket and the lower pocket, respectively. The tool paths are generated by using the contour method provided in Unigraphics®. The pockets with inclined boundary surfaces are machined by using a taper-endmill with 30^o taper angle (b = 30^o) and the cutter radius of r = 0.5". The step-over distance s is 0.5" and the depth of cut d is 0.5". Figures 14(a) and 14(b) show the material engagement and the adaptive feedrate (V_{adp}) control while the cutter is machining the upper pocket along the outer tool path (Figure 13(b)).

Figure 14(c) shows the correspondent machine tool acceleration, a, when the adaptive feedrate (V_{adp}) is applied along the curved tool path. For the given example, the maximum machine acceleration a_{max} is about 7.27 inches/sec^2, which is within the allowable acceleration (a_{max} < 0.3G, as shown in Figure 14(c)). This can be easily achieved on the machine tools for adaptive feed rate control in machining the example part.

Copyright © 2002 by ASME

Downloaded From: https://proceedings.asmedigitalcollection.asme.org on 06/29/2019 Terms of Use: http://www.asme.org/about-asme/terms-of-use

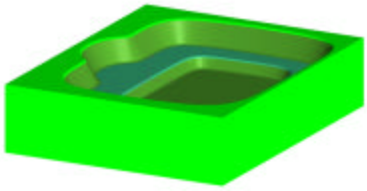

(a) Example part surface with a 30° taper boundary

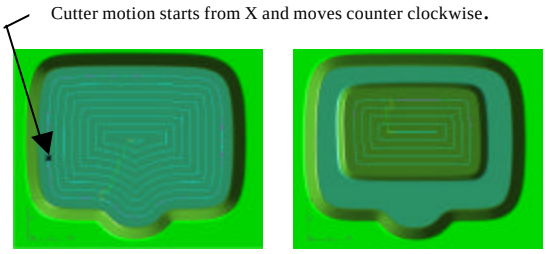

(b) The generated tool path of the upper pocket (c) The generated tool path of the lower pocket

Figure 13. The example part surface and the generated tool paths

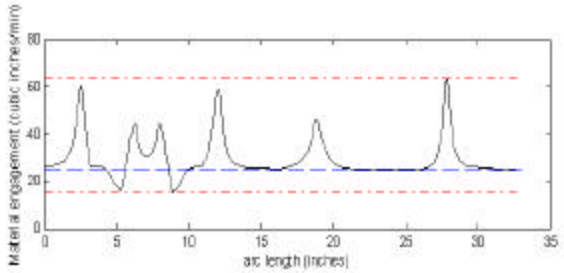

(a) Calculated material removal rate along the curved path

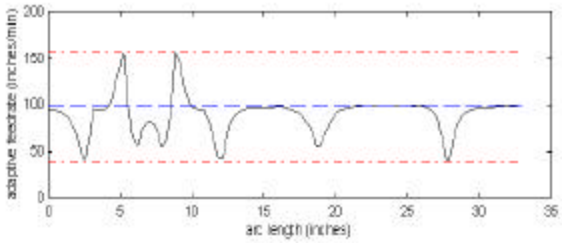

(b) Calculated adaptive feedrate V_{adp} for a constant cutting load

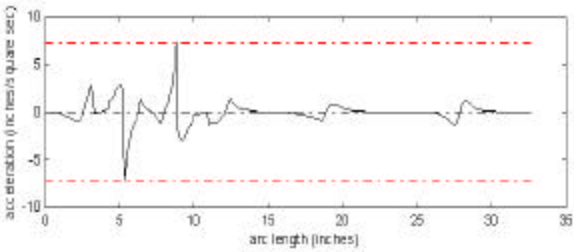

(c) The changing of tangential acceleration along the tool path (a_{max} = 7.27 inches/sec^2 < 0.3 G =115.7 inches/sec^2)

Figure 14. The material engagement, the adaptive feedrate control and the acceleration for machining the example part using a taper-endmil

6 CONCLUSIONS AND DISCUSSION

This paper presents a technique to analyze the instantaneous material removal rate of different endmill cutters moving along either linear or curved tool paths. By analyzing the geometry and the cutting cross-section area of different endmills, the material engagements along either linear motion or curved path motion can be found. To reduce a peak force variation of cutting load along the curved tool paths, one can find and adaptively adjust the corresponding adaptive feedrate to reduce a peak variation cutting load. The techniques developed in this paper can be used in CAD/CAM systems for adaptive feedrate control in tool path generation for 2½D NC machining.

ACKNOWLEDGMENTS

This work was partially supported by the National Science Foundation *CAREER Award* (DMI-9702374) and the Army Research Office (Grant #DAAG55-98-D-0003) to Dr. Y.S. Lee. Their support is greatly appreciated.

REFERENCES

[1] T. E. Bailey, D. M. Jenkins, A. D. Spence, and M. A. Elbestawi, 1996, "Integrated Modeling for Metal Removal Operation," *Proceeding of the ASME Dynamics Systems and Control Division*, **58**, pp. 191-198.

[2] C.E. Becze, P. Clayton, L. Chen, T.I. El-Wardany, and M.A. Elbestawi, 2000, "High-speed five-axis milling of hardened tool steel," *International Journal of Machine Tools & Manufacture*, **40**, pp. 869-885.

[3] Y.H. Chen, Y-S. Lee, and S.C. Fang, 1998, "Optimal Cutter Selection and Machining Plane Determination for Process Planning and NC Machining of Complex Surfaces," *Journal of Manufacturing Systems*, **17(5)**, pp. 371-388.

[4] C.J. Chiou, and Y-S. Lee, 1999, "A shape-generating approach for multi-axis machining G-buffer models," *Computer-Aided Design*, **31(12)**, pp. 761-776.

[5] R. T. Farouki, J. Manjunathaiah, D. Nicholas, G.-F Yuan, and S. Jee, 1998, "Variable-feedrate CNC interpolators removal rates along Pythagorean-hodograph curves," *Computer-Aided Design*, **30(8)**, pp. 631-640.

[6] R.C. Hibbeler, 1974, Engineering Mechanics: Dynamics, Macmillan Publishing Co., Inc.

[7] S.J Huang and C.Y. Shy, 1999, "Fuzzy Logic for Constant Force Control of End Milling," *IEEE Transactions on Industrial Electronics*, **46(1)**, pp 169-176.

[8] W.L.R. Ip, 1998, "A fuzzy basis material removal optimization strategy for sculptured surface machining using ball-nosed cutters," *International Journal of Production Research*, **36(9)**, pp. 2553-2571.

[9] R.B. Jerard, B.K. Fussell, and M.T. Ercan, 2001, "On-Line Optimization of Cutting Conditions for NC Machining," *Proceedings of the 2001 NSF Design, Manufacturing and Industrial Innovation Research Conference*, Jan 7-10, Tampa, Florida, pp. 1-11.

[10] Y. Kakino and A. Matsubara, 1996, "High Speed and High Acceleration Feed Drive System for NC Machine Tools," *International Journal of the Japan Society for Precision Engineering*, **30(4)**, pp. 295-298.

[11] S. Kalpakjian, 1997, "Manufacturing Process for Engineering Materials," *Addison-Wesley Publishing Company*, 3rd Edition.

Copyright © 2002 by ASME

Downloaded From: https://proceedings.asmedigitalcollection.asme.org on 06/29/2019 Terms of Use: http://www.asme.org/about-asme/terms-of-use

[12] J. Kloypayan and Y.-S. Lee, 2002, "Material Engagement Analysis of Different Endmills for Adaptive Feedrate Control in Milling Processes," *Computers in Industry*, **47**, pp. 55-76.
[13] I.H. Kral, 1986, "Numerical control programming in APT," *Englewood Cliffs, N.J.: Prentice-Hall*.
[14] T. Kramer, 1994, "Pocket Milling with Tool Engagement Detection," *Journal of Manufacturing Systems*, **11(2)**, pp. 114-123.
[15] Y-S. Lee and T.C. Chang, 1995, "Application of Computational Geometry in Optimizing 2.5 D and 3D NC Surface Machining, " *Computers in Industry*, **26(1)**, pp. 41-59.
[16] Y-S. Lee, 1998, "Mathematical Modeling Using Different Endmills and Tool Placement Problems for 4- and 5-axis NC Complex Surface Machining," *International Journal of Production Research*, **36(2),** pp. 785-814.
[17] C.C. Lo, 1998, "A new approach to CNC tool path generation," *Computer-Aided Design*, **30(8)**, pp. 649-655.
[18] W.F. Riley and L.D. Sturges, 1993, Engineering Mechanics: Statics, John Wiley & Sons, Inc.
[19] C.A. Rodriguez, 1997, "Ball-nose End Milling Development of Criteria for Automatic Selection of Spindle Speed and Feed Rate," Ph.D. Dissertation of the Ohio State University, Columbus, Ohio.
[20] J.A. Stori and P.K. Wright, 1998, "A Constant Engagement Offset for 2-1/2 D Tool Path Generation," *MED-Vol. 8, Manufacturing Science and Engineering Division*, ASME, pp. 475-481.
[21] S. Takata and M. Tsai, 1994, "Model Based NC Programming for End Milling Operation," *PED-Vol 68-2, Manufacturing Science and Engineering*, **2**, pp. 809-818.
[22] T. M. Tsai, Takata, S., M. Inui, F. Kimura and T. Sata, 1991, "Operation Planning Based on Cutting Process Models," *Annals of the CIRP*, **40(1)**, pp. 95-98.
[23] G. W. Vickers and K. W. Quan, 1989, "Ball-Mills Versus End-Mills for Curved Surface Machining," *Journal of Engineering for Industry*, **111(2)**, pp 22-26.
[24] W. P. Wang, 1988, "Solid Modeling for Optimizing Metal Removal of Three-dimensional NC End Milling," *Journal of Manufacturing Systems*, **7(1),** pp. 57-65.

Authors' Biographical Notes:

Jirawan Kloypayan is a Ph.D. student of the Department of Industrial Engineering at North Carolina State University, USA. She received her B.S. degree in Material Science and M.S. degree in Industrial Engineering from Chulalongkorn University, and her Master degree in Integrated Manufacturing System Engineering from North Carolina State University. Her research interests include computer-aided manufacturing and computational geometry for manufacturing.

Yuan-Shin Lee is an Associate Professor of Industrial Engineering at North Carolina State University, U.S.A. He received his Ph.D. (1993) and MS (1990) degrees from Purdue University, U.S.A., both in Industrial Engineering, and his BS degree from National Taiwan University, Taiwan, in Mechanical Engineering. His research interests include 5-axis sculptured surface manufacturing, CAD/CAM, CAPP, rapid prototyping, and computational geometry for design and manufacturing. He is a registered professional engineer (PE) in mechanical engineering and a certified manufacturing engineer in system integration and control. Dr. Lee received the National Science Foundation *CAREER Award.* He also received the 1997 *Outstanding Young Manufacturing Engineer Award* from the Society of Manufacturing Engineers (SME), the 1998 *Norman Dudley Award* from the Taylor & Francis Editorial Journals, London, U.K., the 1999 *Anderson Outstanding Faculty Award* and the 2000 *Alumni Faculty Outstanding Teaching Award* from North Carolina State University, and the 2001 *ALCOA Foundation Engineering Research Achievement Award*. He serves as an Associate Editor for the *Journal of Manufacturing Systems* (JMS).

Copyright © 2002 by ASME

Downloaded From: https://proceedings.asmedigitalcollection.asme.org on 06/29/2019 Terms of Use: http://www.asme.org/about-asme/terms-of-use